

Article

# Hydrometeorological Ensemble Forecast of a Highly Localized Convective Event in the Mediterranean

Luca Furnari , Giuseppe Mendicino  and Alfonso Senatore \* 

Department of Environmental Engineering, University of Calabria, 87036 Rende (Cosenza), Italy; luca.furnari@unical.it (L.F.); giuseppe.mendicino@unical.it (G.M.)

\* Correspondence: alfonso.senatore@unical.it; Tel.: +39-0984-496614

Received: 18 April 2020; Accepted: 25 May 2020; Published: 28 May 2020



**Abstract:** The uncertainties that affect hydrometeorological modelling chains can be addressed through ensemble approaches. In this paper, a convection-permitting ensemble system was assessed based on the downscaling of all members of the ECMWF ensemble prediction system through the coupled atmospheric-hydrological WRF-Hydro modelling system. An exemplary highly localized convective event that occurred in a morphologically complex area of the southern Italian coast was selected as a case study, evaluating the performance of the system for two consecutive lead times up to the hydrological forecast on a very small (11.4 km<sup>2</sup>) catchment. The proposed approach accurately downscales the signal provided by the global model, improving up to almost 200% the quantitative forecast of the accumulated rainfall peak in the area affected by the event and supplying clear information about the forecast uncertainty. Some members of the ensemble simulations provide accurate results up to the hydrological scale over the catchment, with unit peak discharge forecasts up to 3 m<sup>3</sup>·s<sup>-1</sup>·km<sup>-2</sup>. Overall, the study highlights that for highly localized convective events in coastal Mediterranean catchments, ensemble approaches should be preferred to a classic single-based simulation approach, because they improve the forecast skills and provide spatially distributed information about the forecast uncertainty, which can be particularly useful for operational purposes.

**Keywords:** atmospheric-hydrological forecasting chains; convection-permitting models; ensemble forecasting systems; ECMWF ensemble prediction system; lead time; WRF-Hydro; southern Italy; Mediterranean; coastal systems; convective storms; uncertainty

## 1. Introduction

The coupled weather-hydrological forecasting chains, whose development has undergone a decisive acceleration in recent years, represent potentially invaluable tools for the management of emergencies and civil protection purposes [1] since they allow both the forecast of atmospheric events and the estimate of their hydrological impact on the ground. Nevertheless, both the main components of such complex systems, i.e., the atmospheric and the hydrological models, are subject to so many uncertainties [2,3] that an approach based on single simulations is most often not enough, but it needs to be supported or even replaced by a probabilistic approach based on multiple forecasts (e.g., [4]). The awareness of the high uncertainty lying behind the weather forecasting emerged soon [5], leading to the development of global ensemble prediction systems like, e.g., the Ensemble Prediction System (EPS), which has been operational since 1992 [6] at the European Centre for Medium-Range Weather Forecasts (ECMWF).

The need to estimate in greater detail the extent and intensity of the predicted atmospheric phenomena and the related impact on the ground has been answered by the growing availability of mesoscale models able to perform the dynamical downscaling of forecasts provided by the global models, giving rise to the development of high-resolution ensemble forecasting systems operating at

convection-permitting resolutions [7]. Many studies based on such systems focus on meteorological variables, above all precipitation (e.g., [8–13]). Some other studies incorporate specific aspects (e.g., [14] perturbed the physical parameterizations; [15] and [16] addressed initial conditions perturbations). Nevertheless, increasing examples of coupled ensemble atmospheric-hydrological systems are available, where the Quantitative Precipitation Forecast (QPF) is the main input of the hydrological models (e.g., [17–21]).

Localized highly convective episodes are particularly challenging in terms of both QPF and, consequently, the hydrological response, especially in those regions characterized by a complex orography, where errors of a few kilometers in localizing a given precipitation event, which is still a valuable result in terms of the weather forecast, can provide a rather different hydrological scenario, shifting the flood forecast from one catchment to another. The Mediterranean Basin is a morphologically complex region of the world typically affected by convective episodes, and, in fact, it has been identified as a hot spot of climate change [22], where the intensity and frequency of high-impact weather events are bound to increase [23,24]. In this area, the increasingly complex challenge of efficient and effective hydrometeorological forecasting is also addressed through convection-permitting ensemble forecasting systems (e.g., [25–28]).

The Calabria region at the southern tip of the Italian peninsula, placed in the middle of the Mediterranean Basin, is particularly prone to high-impact episodes, producing noteworthy ground impact with damages and, not seldom, loss of human lives [29]. In this area, the effects of the large gradients between the cooler atmosphere and the warmer sea surface, typical of summer (mainly because of isolated cut-off lows) and autumn (generally connected to frontal systems) seasons, are amplified by the steep orography close to the coast, leading to intense convective precipitation very often characterized by orographic enhancement.

This study aimed to assess the potential benefit of an ensemble approach on the predictability of highly localized convective events in Calabria by analyzing them up to the hydrological-scale impact with a case study that occurred in summer 2015. The analysis was performed using the WRF-Hydro [30] modelling system, composed by the Weather Research and Forecast (WRF) mesoscale model [31], allowing high-resolution (in the order of  $10^3$  m) convection-permitting downscaling of the boundary conditions provided by 50 members of the ECMWF EPS for two consecutive lead times, and its hydrological extension providing detailed information about the impact on the ground at a resolution in the order of  $10^2$  m, which is suitable to medium and small-size catchments' hydrological modelling. Therefore, a case study concerning a complete hydro-meteorological ensemble forecasting chain is proposed, where the uncertainty is accounted only for the atmospheric modelling, and then cascaded throughout the forecasting chain. This choice is explained both by the fact that the meteorological input is generally supposed to be the main source of uncertainty in short-range hydrological forecasts (even though this assumption is debatable, according to [32]) and by the purpose of clearly highlighting, for the sake of clarity, only the effects of the meteorological uncertainty, evaluating also its magnitude with different forecast lead times.

The described research followed and aimed to integrate a previous analysis already performed for the same event [33], which showed the limits of a single-based simulation approach, even supported by variational data assimilation techniques, for the accurate predictability of both the meteorological and hydrological features. Specifically, among the different mesoscale model boundary conditions investigated in [33], the most suitable were selected and used as a starting point for the analysis shown in this paper. Therefore, the choice of the summer 2015 event is justified by a combination of features that makes it almost unique in the analyzed region, since it is: (1) A relatively recent high-impact event (with almost 250 mm of rain in 24 h); (2) a highly localized event, whose signal was recorded by only one weather station of the dense Calabrian monitoring network; and (3) an already well-studied event, simulated with varying boundary conditions and with/without data assimilation techniques. These features allow it to be considered as an exemplary case study, from which general conclusions, applicable to similar events, can be drawn.

In the following, Section 2 describes the study area and the weather event analyzed and provides details about the modelling approach and the validation strategy. Section 3 shows the results of the coupled meteo-hydrological analysis, while Section 4, finally, discusses the main findings achieved, summarizes the main conclusions, and provides insights for future research.

## 2. Materials and Methods

### 2.1. Study Area and Modelling Approach

Calabria is the southernmost Italian peninsula (Figure 1), surrounded by the Tyrrhenian Sea (western coast) and the Ionian Sea (southern and eastern coast). Despite its proximity to the sea, more than 40% of its total area of about 15,000 km<sup>2</sup> is higher than 500 m above the sea level (a.s.l.). The orographic features play a fundamental role in the development of high-impact events, hitting especially (but not exclusively) the eastern coast [34–39].

The limited area model (LAM) used in this study is the Weather Research and Forecasting—Advanced Research (WRF-ARW, [31]) version 3.7.1, with two one-way nested domains (Figure 1), whose main properties are shown in Table 1. The same table also reports the physics parameterization of the mesoscale model (which is the same used by [33,40]), together with information about the initial and boundary conditions (ICs and BCs, respectively) provided by the high-resolution simulation and both the ensemble control and member simulations of the reference Global Circulation Model (GCM). Considering the problems related to the spatial interpolation of the Sea Surface Temperature (SST) variable arisen with the ECMWF-EPS, which were also found in previous studies [33,39], Table 1 also provides information about the lower (SST) initial and boundary conditions used.

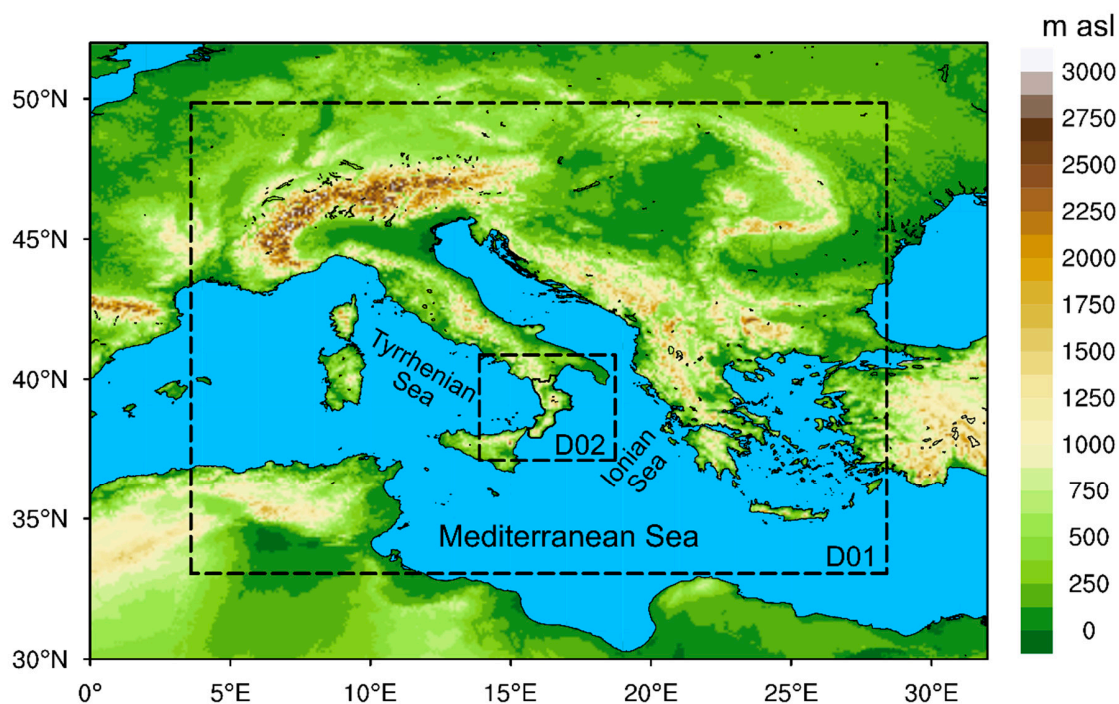


**Figure 1.** WRF computational domains (dashed lines). The outermost domain D01 is centered over the central Mediterranean Sea, and the innermost D02 is centered over the Calabria region, whose northern border is highlighted with a black bold line.

**Table 1.** Main features of the simulations performed in this study.

<b>WRF Physics Parameterization</b>	
<i>Component</i>	<i>Scheme</i>
Microphysics	Lin-Purdue [41]
PBL	MJY [42]
Shortwave Radiation	Dudhia [43]
Longwave Radiation	RTTM [44]
Land Surface Model	Unified NOAH [45]
Surface Layer	Eta Similarity [46]
Cumulus	Kain-Fritsch (D01) [47]
<b>WRF Domains Space and Time Resolutions</b>	
D01	10 km (205 × 187 grid points), 60 s
D02	2 km (200 × 200 grid points), 12 s
Vertical layers	44 terrain-following layers above the surface and 4 layers in the soil
<b>WRF Initial and Boundary Conditions (ICs and BCs)</b>	
GCM ICs and BCs	ECMWF-EPS, reference IFS Cycle 41r1 [48]
HRES:	High-resolution simulation at 16 km resolution
LRES_CON:	Ensemble control simulation at 32 km resolution
LRES_ENS:	50 perturbations are applied to the initial conditions of the GCM, based on a multivariate Gaussian sampling technique [49]
Lower BCs (SST)	Native SST fields replaced with the Medspiration L4 Ultra-High Resolution SSTnd product as a daily mean at a resolution of 0.022° [50,51]. The <i>sst_update</i> and the <i>sst_skin</i> [52] options were also activated, which permit dynamic SST and allow the system to simulate the daily SST cycle, respectively
<b>WRF-Hydro Main Features</b>	
Land Surface Model	Unified NOAH, 2 km resolution
Active modules	Subsurface, surface and channel water routing
Input from WRF	Precipitation and pressure on the ground, air temperature and humidity, wind speed and solar radiation (1 h time step)
Resolution	200 m (2000 × 2000 grid points), disaggregation factor with respect to the atmospheric model of 1/10
<b>Initialization Time and Range of the Simulations</b>	
0000 UTC	0000 UTC 11 August 2015 (48 h range)
1200 UTC	1200 UTC 11 August 2015 (36 h range)

The atmospheric-hydrologic modelling chain was completed by the WRF Hydrological (WRF-Hydro) modelling system version 3.0 [30], used in one-way mode (i.e., without considering any feedback to the atmosphere of the surface and subsurface water routing operated by the hydrological model). WRF-Hydro is a model coupling framework designed to link multi-scale process models of the atmosphere and terrestrial hydrology [53], which allows the mesoscale model to be connected to a semi-distributed hydrological model. In its turn, the latter couples a monodimensional land-surface scheme to algorithms allowing the two-dimensional horizontal flow of the water over the land surface and in the subsurface layers, groundwater models, and flow routing models along the channel. Both one-way and fully-coupled versions of WRF-Hydro have been successfully tested in the Mediterranean region with both short-term and long-term simulations (e.g., [54–56]). In this study, due to the short duration of the event analyzed, the groundwater model was not activated. More information about the WRF-Hydro modelling details for this study is provided in Table 1.

## 2.2. Case Study

The analyzed case study concerns intense and rather localized precipitation that occurred in the first hours of 12 August 2015 and affected almost only a small area in the north-eastern side of the region (Figure 2a), corresponding to the municipalities of Corigliano Calabro and Rossano [57]. The synoptic

analysis shows that the event was due to a cut-off low generated over the Atlantic, which reached the central Mediterranean some days after, entailing the advection of the convective cells that developed over the Ionian Sea towards the impacted area, corresponding broadly to the coast and the first slopes of the Sila Plateau (Figure 2b). Figure 2a shows the spatial distribution of rainfall observations on the ground provided by the Centro Funzionale Multirischi—ARPACAL of the Calabria Region and detected by the radar network managed by the National Civil Protection for 24 h between 1800 UTC on 11 August 2015 and 1800 UTC on 12 August 2015. It is noteworthy that the Corigliano rain gauge recorded 246.6 mm in 24 h, of which 223.2 mm in only 12 h, corresponding to a return-time period of 151 years, and 167.4 mm in 6 h, corresponding to a return-time period of 179 years (Figure 2c). The starting times selected for the two ensemble simulations performed in the study were 0000 UTC and 1200 UTC on 11 August 2015 (Table 1), allowing lead times of about one day and half-day, respectively, to the time when the highest rainfall intensity started.

Among the several small and very small catchments affected by the event, the most relevant hydrological impact concerned the Citrea creek, a small coastal catchment extending for only 11.4 km<sup>2</sup> (Figure 2b). The length of the creek is 9.6 km, while the basin has an average elevation of 236 m a.s.l. (maximum elevation of 785 m a.s.l.), an average slope of 9.6%, and a lag time estimated between 15 and 20 min. According to the Corine Land Cover 2018 project [58], about 28% of the catchment area is covered by artificial surfaces, 49% by agriculture areas, and the remaining 23% by forest and semi-natural areas. Unfortunately, neither discharge nor hydrometric observations are available for the Citrea creek; therefore, the hydrological model was not calibrated and the default parameterization was chosen, which, however, was enough for the aims of this study, whose objective was to explore the added value of an ensemble forecasting chain to the predictability of the event rather than estimating specific hydrological quantities, such as, e.g., peak flow.

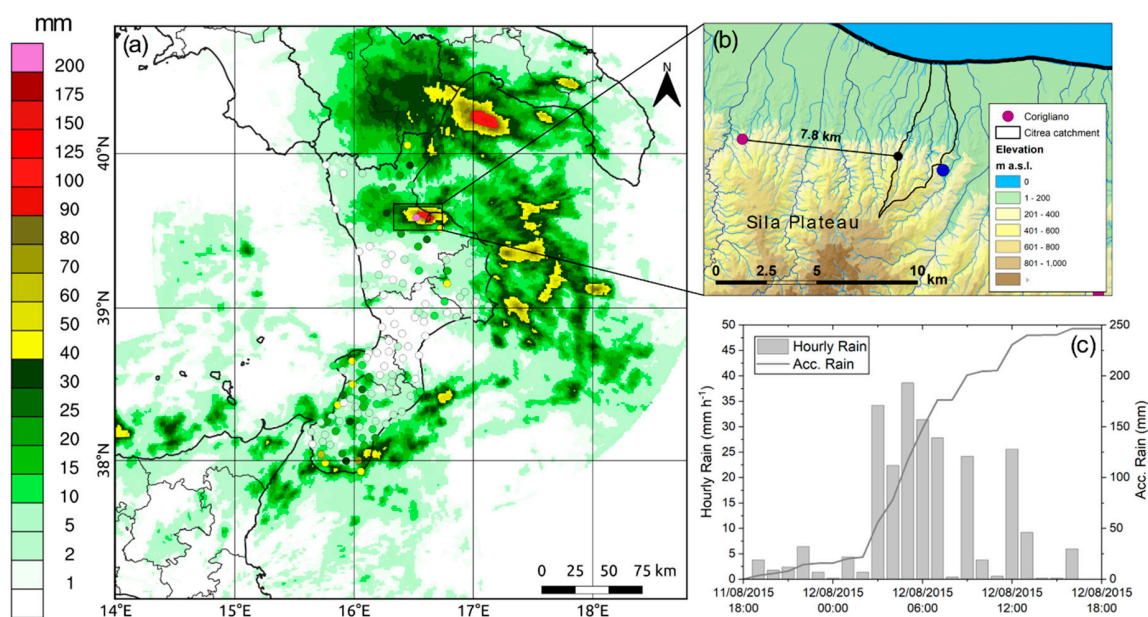


**Figure 2.** (a) The accumulated precipitation observed by the regional monitoring network (dots), overlying the meteorological radar observations during the interval between 1800 UTC, 11 August 2015 and 1800 UTC, 12 August 2015; regional borders are shown together with the coastlines; (b) zoom of the study area highlighting both the local orography and river network, which shows a distance lower than 8 km between the Citrea creek catchment and the Corigliano rain gauge; the location of the municipality of Rossano (old city) is indicated with a blue point; (c) cumulative and hourly observed hyetograph (mm) at the Corigliano rain gauge.

### 2.3. Validation Strategy

Given the peculiarity of the event, which essentially interested only one rain gauge, the performances of the 51 (50 ensemble members and the control run) weather simulations for each of the two ensemble forecasts were assessed, developing a tailored approach.

Concerning the spatial pattern of the simulated precipitation, the rainfall fields produced by the ensemble members were accumulated over 24 h, performing later over the whole domain D02 a cell-by-cell statistical analysis, which led to maps of the mean values, standard deviation, and different percentiles. Such analysis allowed, in particular, the spatial variability of uncertainty to be highlighted.

Concerning the comparison with observed rainfall in the analyzed area (i.e., with the observations at the Corigliano rain gauge), since radar data underestimate observations and the event is extremely localized, the analysis focused on a square box with an 80 km side (i.e., 1600 grid points), centered on the Corigliano rain gauge and including the Citrea creek catchment. Within this box, for each weather simulation, the maximum cumulative value over 24 h and its position within the domain D02 was identified and, for the relative grid point, the rainfall time series was extracted.

Finally, concerning the evaluation of the hydrological impact, for each ensemble member, the averaged precipitation amount over the Citrea creek catchment was assessed. Furthermore, the discharge series calculated by the WRF-Hydro model, starting from initial conditions provided by the ERA-Interim [59] reanalysis, were evaluated in terms of the peak flow time and hydrograph shape.

## 3. Results

### 3.1. Meteorological Ensembles

Though its increasingly higher detail, the ECMWF Integrated Forecasting System (IFS) does not provide an adequate spatial resolution (both as high-resolution and ensemble forecasts) for capturing highly localized convective episodes, such as that analyzed. Table 2 shows for the two starting times of the simulation (0000 UTC and 1200 UTC on 11 August 2015, respectively) that, if the precipitation rate is evaluated for a relatively wide area equal to the innermost domain, the amounts estimated by the GCM and the LAM are comparable (starting time 0000 UTC) or even the GCM amount is significantly higher than the LAM (starting time 1200 UTC). Nevertheless, if the analysis is tightened around the Corigliano rain gauge, the GCM cannot provide realistic information, estimating rainfall peaks equal about from one-third to one-half of those provided by the mesoscale model and from one-tenth to one-seventh of that observed (with starting time 0000 UTC and 1200 UTC, respectively). In particular, in both the forecasts, only 2 out of the 50 members of the ensembles estimate accumulated rainfall amounts to close to  $100 \text{ mm} \cdot 24 \text{ h}^{-1}$ , while 29 and 15 members, with a starting time of 0000 UTC and 1200 UTC, respectively, do not reach  $30 \text{ mm} \cdot 24 \text{ h}^{-1}$ . The GCM underestimations are tightly connected to its coarser resolution compared to the LAM, which both averages precipitation values over larger grid areas (i.e., from  $2^2$  to  $16^2$  or  $32^2 \text{ km}^2$ ) and, mainly, flattens the complex orography simplifying the morphological features of the area. Therefore, a downscaling approach, either statistical or (such as in this case study) dynamical, is unavoidable.

Focusing on the WRF downscaled forecasts, it is noteworthy that the average value of the rainfall peaks of the ensemble forecast near the Corigliano rain gauge increase of about 30% from the first (0000 UTC) to the second (1200 UTC) forecast, while the high-resolution and low-resolution control simulations peaks slightly decrease.

Figures 3 and 4 relate to forecast starting times of 0000 UTC and 1200 UTC, respectively, and provide outlooks on the overall behavior of the downscaled ensemble simulations. Concerning the forecast starting at 0000 UTC, the low-resolution control simulation (Figure 3a) forecasts some relevant rainfall peaks both over the Ionian sea (at about the coordinates  $39^\circ \text{ N}$ ,  $18^\circ \text{ E}$ ; about 130 km from the centroid of the Citrea creek) and over the land, on the Tyrrhenian coast (about  $39^\circ \text{ N}$ ,  $16^\circ \text{ E}$ ; about 70 km from the Citrea creek) and on the northern (near the location where the event actually occurred) and southern Ionian coastline. In the latter location (about  $38.5^\circ \text{ N}$ ,  $16.5^\circ \text{ E}$ ; about 110 km from the

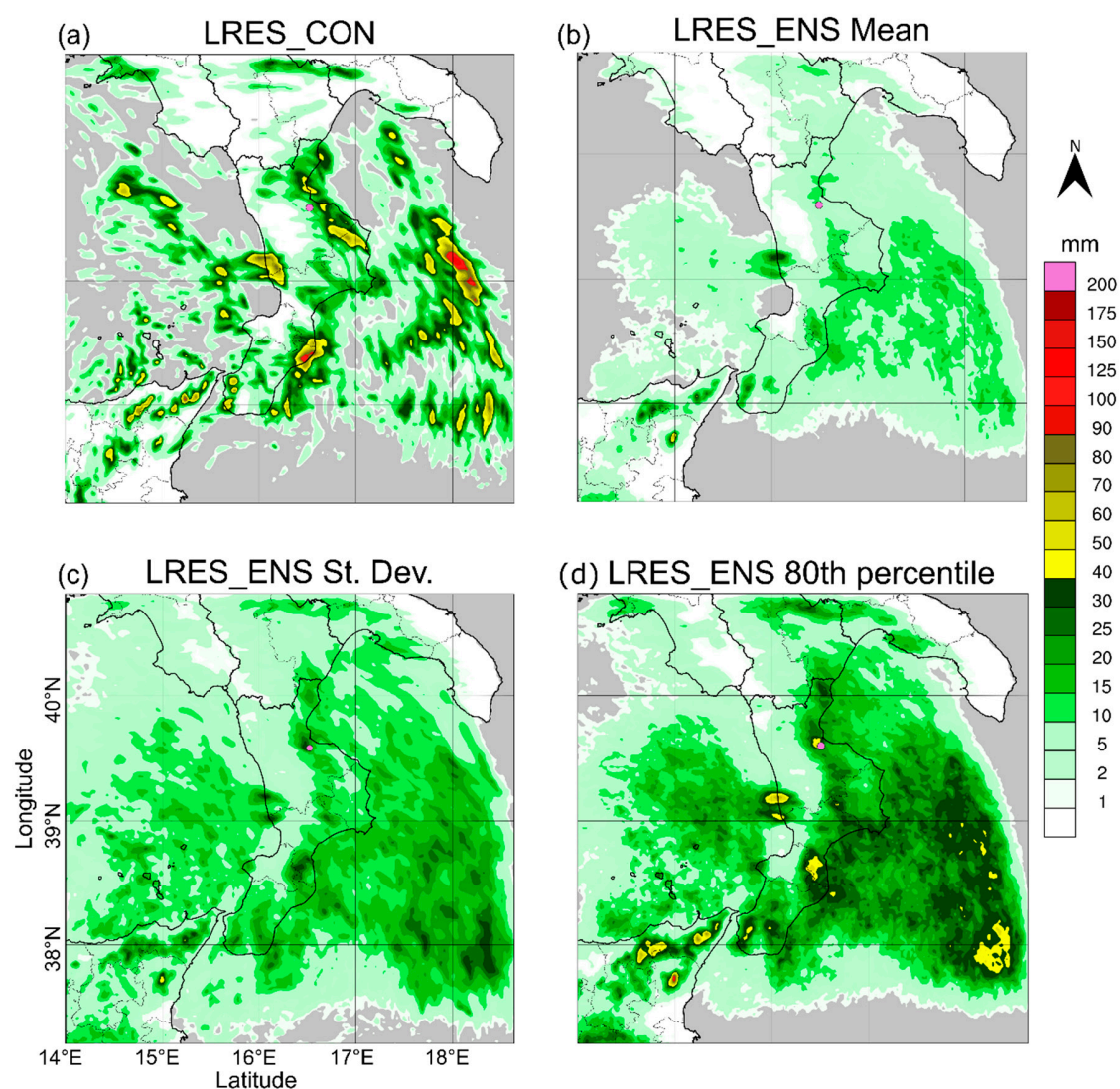
Citrea creek), the highest rainfall peak over the land ( $>100 \text{ mm}\cdot 24 \text{ h}^{-1}$ ) is forecasted, not corresponding, however, to the observations (Figure 2a). The ground monitoring network highlights noteworthy accumulated precipitation ( $>40 \text{ mm}$ ), besides the Corigliano area, only along the southern Tyrrhenian coast and at the southernmost bottom of the peninsula. The control simulation of the ensemble forecast starting at 1200 UTC (Figure 4a) does not provide more detailed information, showing a bit drier pattern over the northern Ionian coast. Both in the 0000 UTC and 1200 UTC forecasts, each of the 50 perturbed simulations shows rainfall patterns like the respective low-resolution control simulations, with localized peaks especially in the eastern side of the domain. However, while in the 0000 UTC forecast, on average, no particularly intense rainfall is expected (the pattern in Figure 3b is explained by the fact that the locations of the rainfall peaks forecasted by the ensemble simulations are rather scattered), some more detailed information is given by Figure 4b, relating to the 1200 UTC forecast, where some rainfall peaks are more evident. The highest mean values in the 0000 UTC forecast are found along the Tyrrhenian coastline where the low-resolution control simulation erroneously forecasts rainfall rates of about  $70\text{--}80 \text{ mm}\cdot 24 \text{ h}^{-1}$ . The same peak (more intense) is found in the 1200 UTC forecast, together with another one in the south of the region. The standard deviation maps (Figures 3c and 4c) are more interesting since they account directly for the forecast uncertainty. Over the land, the highest standard deviation values are found roughly in the same locations where the low-resolution control simulations forecast the highest peaks, i.e., on the Tyrrhenian coast (about  $39^\circ \text{ N}$ ,  $16^\circ \text{ E}$ ; about 70 km from the Citrea creek), the southern Ionian coast (about  $38.5^\circ \text{ N}$ ,  $16.5^\circ \text{ E}$ ; about 110 km from the Citrea creek), and where the analyzed event occurred, i.e., in the Corigliano area. The high standard deviation entails higher rainfall rates in the percentile maps. As an example, the 80th percentile map in Figure 3d shows, together with a couple of incorrectly forecasted peaks (on the Tyrrhenian and southern Ionian coasts, respectively), that intense rainfall is correctly forecasted both in the extreme south of the peninsula and, mainly, in the Corigliano area, even though at rates still considerably lower than observations. Figure 4b confirms the same behavior in the 1200 UTC forecast, with higher rainfall amounts.

**Table 2.** Average accumulated precipitation in the innermost domain and rainfall peak in an 80 km-side square box centered on the Corigliano rain gauge in the period 1800 UTC, 11 August 2015—1800 UTC, 12 August 2015, forecasted by ECMWF IFS and WRF. Units are in ( $\text{mm}\cdot 24 \text{ h}^{-1}$ ). HRES: high-resolution simulation; LRES\_CON: low-resolution ensemble control simulation; LRES\_ENS: low-resolution ensemble simulations.

Variable	ECMWF IFS			WRF		
	HRES	LRES_CON	LRES_ENS	HRES	LRES_CON	LRES_ENS
Starting time 11 August 2015 0000 UTC						
Average accumulated precipitation in D02	9.3	8.5	$10.6 \pm 3.4$	$9.5^1$	6.6	$6.7 \pm 2.0$
Rainfall peak near Corigliano	22.9	27.4	$31.0 \pm 22.2$	$73.7^1$	80.3	$87.2 \pm 35.4$
Starting time 11 August 2015 1200 UTC						
Average accumulated precipitation in D02	12.7	12.1	$12.0 \pm 2.7$	7.0	7.0	$7.3 \pm 1.1$
Rainfall peak near Corigliano	39.3	35.1	$41.4 \pm 18.7$	63.7	70.9	$112.9 \pm 40.0$

<sup>1</sup> results from [33].

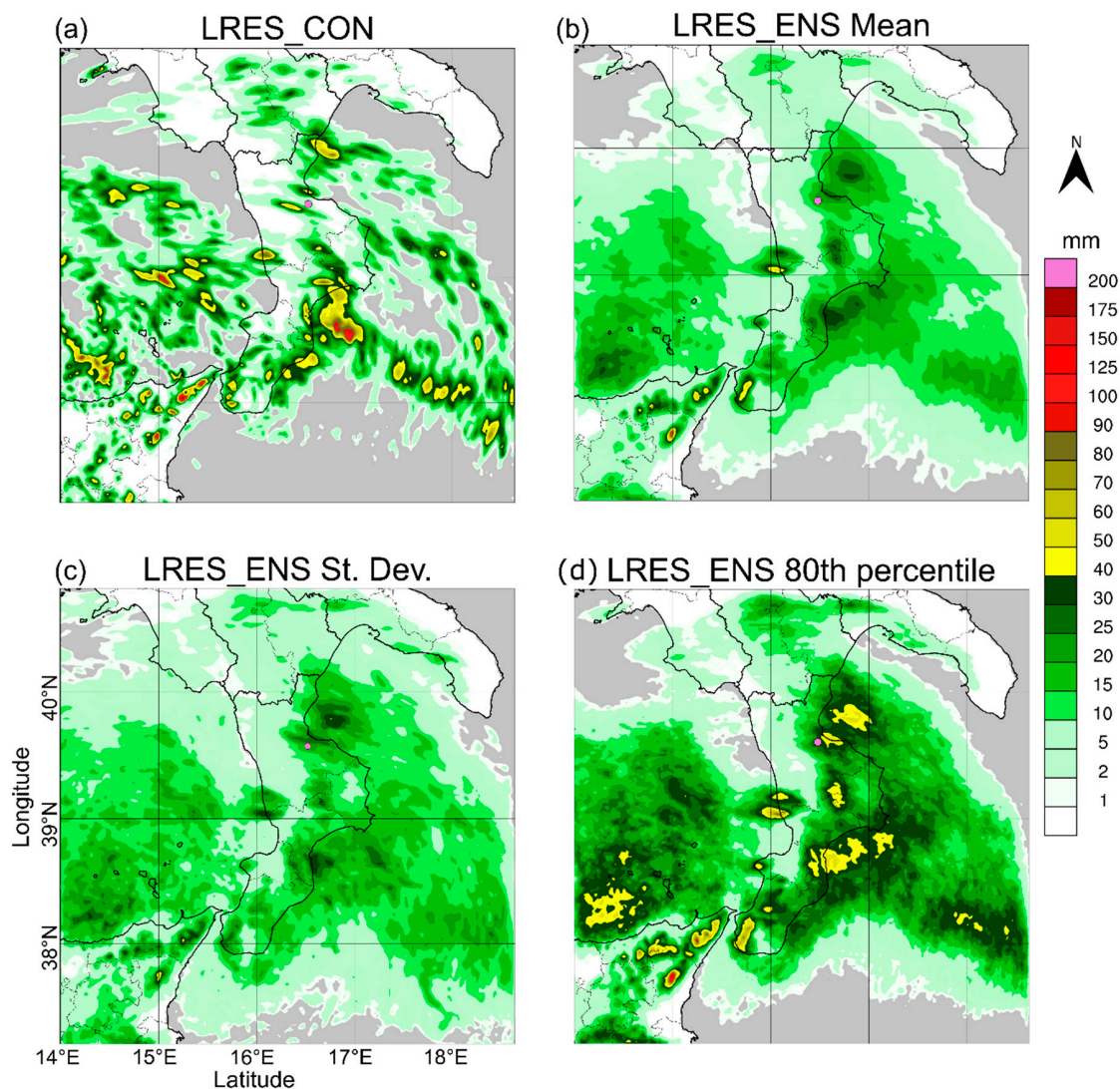
Therefore, the spatial analysis of the high-resolution ensemble forecasts over the whole region highlights that, though some false alarms are identified, a signal of the upcoming extreme event on the Corigliano area is detected.



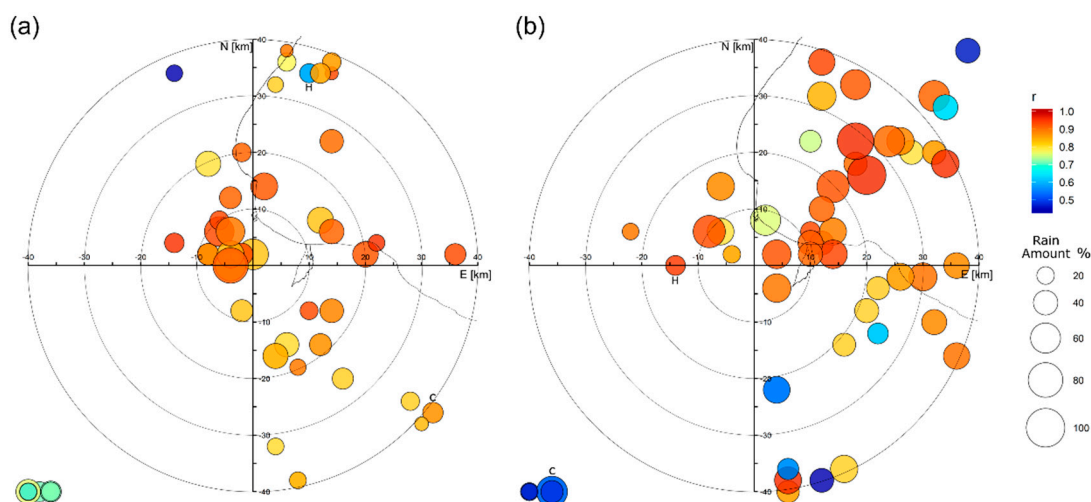
**Figure 3.** Accumulated precipitation (mm) simulated by WRF using the ECMWF EPS boundary conditions (simulation start at 0000 UTC, 11 August 2015) during the 24-h-long period 1800 UTC, 11 August 2015—1800 UTC, 12 August 2015: (a) low-resolution control simulation; (b) cell-by-cell mean of the 50 perturbed forecasts, (c) same as (b), but for standard deviation; (d) same as (b), but for the 80th percentile. The colored dot represents the Corigliano gauge station.

Focusing on the Corigliano area, both the performances in space and time of the ensemble forecasts are assessed through the graphs in Figures 5 and 6. Specifically, Figure 5 summarizes the location, the 24-h accumulated value, and its time correlation with observations for each of the rainfall peaks simulated by the 50 perturbed simulations of both the 0000 UTC and 1200 UTC forecasts, together with the respective low-resolution control and the high-resolution simulations, within an 80 km-side squared box centered on the Corigliano rain gauge. To avoid detecting insignificant peaks, a lower threshold of 30 mm was assumed. Almost all the simulations forecast noteworthy rainfall peaks within the considered squared area. The peaks are detected at the border of the box (since they belong to rainfall clusters having their maximum values outside the box itself) only for nine (5) simulations in the 0000 UTC (1200 UTC) forecast. These peaks are represented in the circles mainly gathered on the bottom-left sides of both Figure 5a,b. As it is clear from Table 2, all simulations underestimate the observations (their amount is  $35.4 \pm 14.4\%$  and  $45.8 \pm 16.2\%$  of the rain gauge value on average, for the 0000 UTC and 1200 UTC forecasts, respectively), yet they are quite correlated (Pearson's correlation coefficient  $r = 0.85$  for the 0000 UTC and  $r = 0.91$  for the 1200 UTC forecast). In both the forecasts, the low-resolution control

and the high-resolution simulations do not show particularly high performances, especially concerning the rainfall amount. Since the low-resolution control simulation is equal to the high-resolution except resolution, the distances between the peaks related to the high-resolution and the low-resolution control simulations highlight that the effect of the boundary conditions is not negligible. On the other hand, the relatively low performances of the high-resolution forecasts (especially with the 0000 UTC starting time) highlight that, in this case, the higher resolution of the boundary conditions (i.e., 16 vs. 32 km) does not provide a clear benefit to the forecast accuracy. This result can be related to the chaotic nature of the precipitation pattern in the convective event, where other sources of uncertainty overwhelm the potentially positive effect of higher resolution boundary conditions. It is noteworthy that the precipitation variability in the innermost domain is highly enhanced by the resolution of the mesoscale model. For example, the correlation coefficient  $r$  between the accumulated rainfall peak around Corigliano and the averaged accumulated rainfall in the whole domain is equal to 0.68 (0.42) for the EPS but only to 0.02 (0.11) for the downscaled ensemble in the 0000 UTC (1200 UTC) forecast.



**Figure 4.** Accumulated precipitation (mm) simulated by WRF using the ECMWF EPS boundary conditions (simulation start at 1200 UTC, 11 August 2015) during the 24-h-long period 1800 UTC, 11 August 2015—1800 UTC, 12 August 2015: (a) low-resolution control simulation; (b) cell-by-cell mean of the 50 perturbed forecasts, (c) same as (b), but for standard deviation; (d) same as (b), but for the 80th percentile. The colored dot represents the Corigliano gauge station.



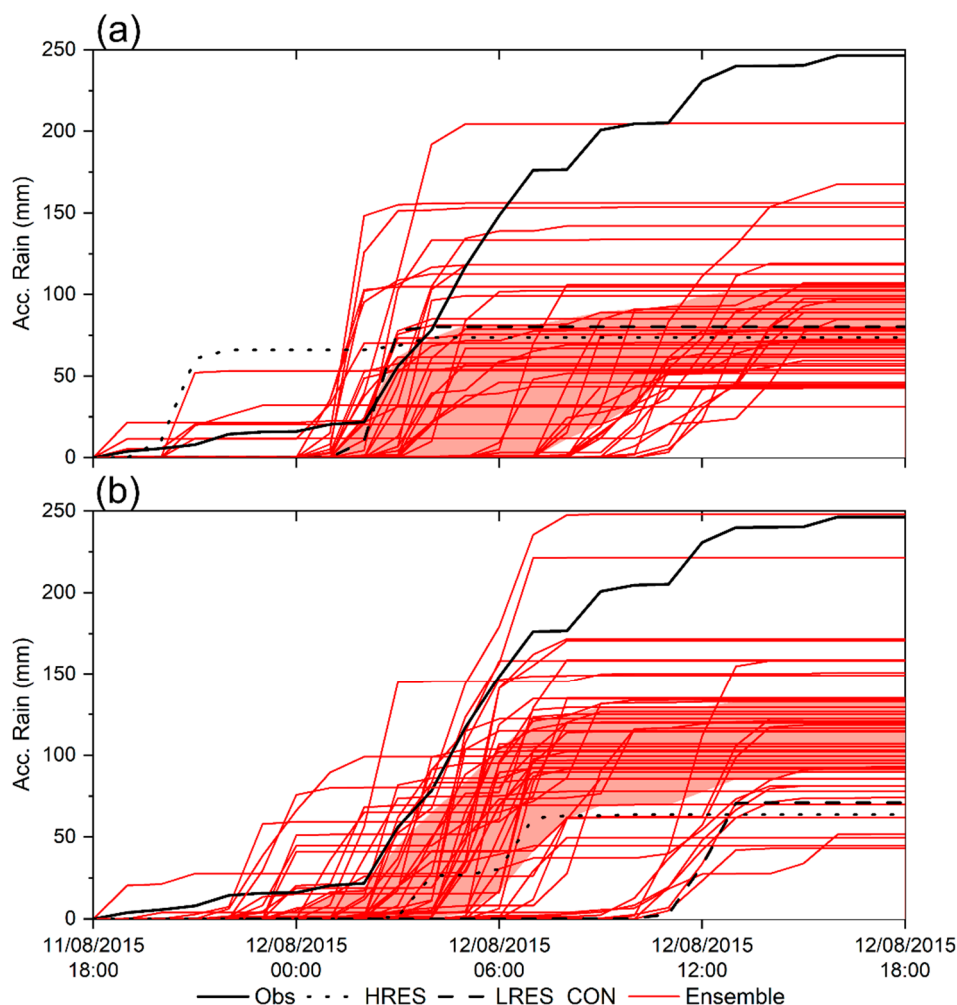
**Figure 5.** Location of the rainfall peaks within an 80 km-side squared box centered on the Corigliano rain gauge for the high-resolution forecast (letter “H” inside the circle), the low-resolution control forecast (letter “C”), and the 50 perturbed simulations, for the forecasts starting at (a) 0000 UTC and (b) 1200 UTC on 11 August 2015. The colors represent the time correlation of the series of accumulated precipitation with observations ( $r$  is the correlation coefficient), while the size indicates the percentage rainfall amount with respect to observations. The circles on the bottom-left and upper-right corners account for the perturbed forecasts with rainfall peaks at the border of the boxes. The borders of the Citrea creek catchment are also represented.

Figure 5 highlights different patterns for the locations of the highest accumulated rainfall peaks in the 0000 UTC and 1200 UTC forecasts. In the former, most of the highest peaks are quite close to Corigliano. Specifically, of the 10 highest peaks, 8 are less than 15 km away and 6 less than 10 km. The peak of the simulation providing the highest rainfall amount (the ensemble member no. 36, with  $204.8 \text{ mm}\cdot 24 \text{ h}^{-1}$ ) is located only 4 km west of the gauge station. On the other hand, the peaks of the 1200 UTC forecast (Figure 5b) are generally biased towards the north-east quadrant (52% of the members, including 10 out of the 12 highest peaks) but some of them are capable of affecting the Citrea catchment.

The spaghetti graphs shown in Figure 6 goes into details concerning the time correlation of both the observed and forecasted accumulated precipitation values in the Corigliano area. While they confirm the general underestimation of the ensemble forecasts (the observed time series overlay the first to third quartile bands only at the very beginning of the event) and the not high performances of the high-resolution and low-resolution control forecasts, they also highlight the reasonable behavior of some ensemble members. In particular, for the forecast starting at 0000 UTC, the rainfall time series of the member no. 36 (i.e., the red line with the highest accumulated rainfall value in Figure 6a) reaches an accumulated value equal to 83% of the observations and is highly correlated ( $r = 0.92$ ). Members no. 34 and no. 39 of the ensemble forecast starting at 1200 UTC provide even higher rainfall peaks (Figure 6b), with  $248.0$  and  $221.5 \text{ mm}\cdot 24 \text{ h}^{-1}$ , respectively ( $r = 0.98$  in both cases). Nevertheless, these peaks are located relatively far from the Corigliano rain gauge, both about 26–28 km north-east, hence the very localized rainfall pattern does not reach the mainland (not shown).

The overall high indices of the member no. 36 of the ensemble forecast starting at 0000 UTC suggest a further more detailed analysis of this simulation. Figure 7 shows its forecasted 24-h accumulated precipitation map from 1800 UTC, 11 August 2015 to 1800 UTC, 12 August 2015. The rainfall spatial pattern is slightly different from that detected by the low-resolution control simulation (Figure 3a). The precipitation amount increases considerably in the eastern side of the domain, over the Ionian Sea, while it reduces over the western side. This behavior is a consequence of several differences in the atmospheric features caused by the boundary conditions provided by the EPS member no. 36: More

humid and warmer air is advected over the Ionian Sea, with integrated water vapor values of up to  $50 \text{ kg}\cdot\text{kg}^{-1}$  and higher potential temperature (up to about 292 K at 850 hPa) during the night (maps not shown), entailing higher convective available potential energy (CAPE) values (over  $3500 \text{ J}\cdot\text{kg}^{-1}$  offshore the Ionian coast). Overall, the forecast provided by the ensemble member no. 36 looks more coherent than the low-resolution control simulation with radar observations (e.g., the model can simulate the rainfall peak detected by the radar in the northern part of the Ionian Sea shown in Figure 2a).



**Figure 6.** Spaghetti graphs of the accumulated rainfall peaks around the Corigliano rain gauge shown in Figure 5: (a) forecasts starting at 0000 UTC, 11 August 2015; (b) forecasts starting at 1200 UTC, 11 August 2015. The light red bands highlight the intervals between the 1st and the 3rd quartiles. The dotted line indicates the HRES simulation, while the dashed line is the low-resolution EPS control simulation.

Over the land, the rainfall overestimation in the central-southern Ionian coast, already highlighted in the ensemble low-resolution control simulation, is more widespread, while an opposite behavior is observed for the overestimation in the Tyrrhenian coast (i.e., the extent of the area with over-forecasted precipitation is reduced compared to the low-resolution control simulation). The main change, however, occurs in the Corigliano area, where the scattered rainfall clusters simulated in the low-resolution control simulation are gathered into a more intense one, which is centered almost exactly on the rain gauge station. Nevertheless, the rainfall cluster is so highly concentrated in space that it does not include the Citrea creek catchment. Indeed, in the analyzed 24-h interval, the ensemble member no. 36 forecasts only about 1 mm of averaged precipitation over the Citrea creek catchment area. The high

performance of the precipitation forecast at the Corigliano rain gauge does not lead to an improved hydrological simulation in a catchment only 8 km away from the rain gauge itself.

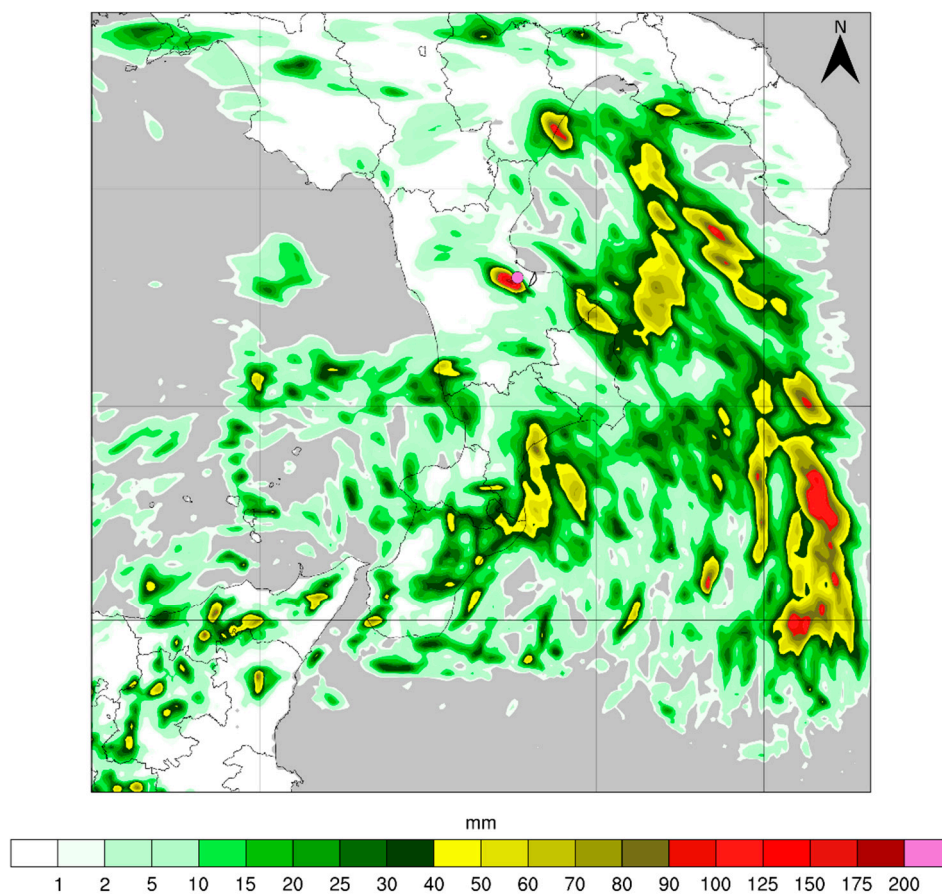


**Figure 7.** 24-h accumulated precipitation (mm) simulated by WRF using the boundary conditions from the ECMWF EPS perturbed forecast no. 36 (from 1800 UTC, 11 August 2015 to 1800 UTC, 12 August 2015; starting time of the forecast 0000 UTC, 11 August 2015). The colored dot highlights the Corigliano's rain gauge station. The borders of the Citrea creek catchment are also represented.

### 3.2. Hydrological Ensembles

Figure 8 shows the hourly accumulated rainfall averaged over the Citrea creek catchment and the resulting hydrographs achieved with the WRF-Hydro model using the ensemble low-resolution control simulation and the 50 perturbed ensemble simulations in the 0000 UTC and 1200 UTC forecasts. Both the highest 24-h accumulated rainfall and the highest hourly rainfall intensity in the 0000 UTC forecast are provided by the ensemble member no. 16 (58.8 and 39.8 mm·h<sup>-1</sup> between 0200 and 0300 UTC, respectively). The 24-h rainfall peak of this simulation within the 80 km-side squared box centered on the Corigliano rain gauge is 112.6 mm·24 h<sup>-1</sup> and is localized not far from the Citrea creek (about 12 km to the east and 8 to the north of the Corigliano station). In the 1200 UTC forecast, the ensemble member no. 47 provides the highest accumulated rainfall amount (78.0 mm·24 h<sup>-1</sup>) and almost the highest hourly intensity (57.4 mm·h<sup>-1</sup> between 0600 and 0700 UTC), only slightly exceeded by the member no. 21 (57.8 mm·h<sup>-1</sup>, again between 0600 and 0700 UTC). The 24-h rainfall peaks of both these simulations are rather far from the Citrea creek (from 25 to 30 km).

Notwithstanding the likely underestimation of the accumulated precipitation (it is worth reminding that the Corigliano rain gauge recorded 223.2 mm in only 12 h), the hourly intensity peak of about 40 mm·h<sup>-1</sup> of the ensemble member no. 16 (0000 UTC forecast) is comparable to that observed

(Figure 2c) and is timely, while the highest hourly intensities of the ensemble members of the 1200 UTC forecast are even higher (almost  $60 \text{ mm}\cdot\text{h}^{-1}$ ) but late.

The ensemble member no. 16 of the 0000 UTC forecast leads to a low peak flow (about  $3.4 \text{ m}^3\cdot\text{s}^{-1}$ , Figure 8a), even with a sufficiently high simulated rainfall intensity peak. On the other hand, in the ensemble forecast starting at 1200 UTC, much higher values are reached (up to  $30 \text{ m}^3\cdot\text{s}^{-1}$ , Figure 8b), which, though lower than the peak flow of about  $90 \text{ m}^3\cdot\text{s}^{-1}$  estimated by the ARPACAL Agency [57] (and it makes sense, given the overall underestimation of the accumulated precipitation), is enough for triggering early warning measures for that specific catchment.

Even neglecting the problems due to the missed calibration, which can influence the peak discharge value, it is noted that the aforementioned simulations provide almost all isolated rainfall peaks, producing a rather impulsive response of the catchment. On the other hand, the observed hyetograph (Figure 2c), though relative to a site slightly out of the catchment, highlights five consecutive hours (from 0200 to 0700 UTC) with an average intensity over  $30 \text{ mm}\cdot\text{h}^{-1}$ , suggesting that no simulation can correctly reproduce the persistence of the precipitation event over the Corigliano area. Furthermore, even with comparable hyetographs, the spatial distribution of the simulated precipitation within the catchment area should also have been carefully evaluated, given the sharp differences in land use between the upper (mainly rural) and lower (urbanized) areas of the catchment, entailing rather different hydrological responses.

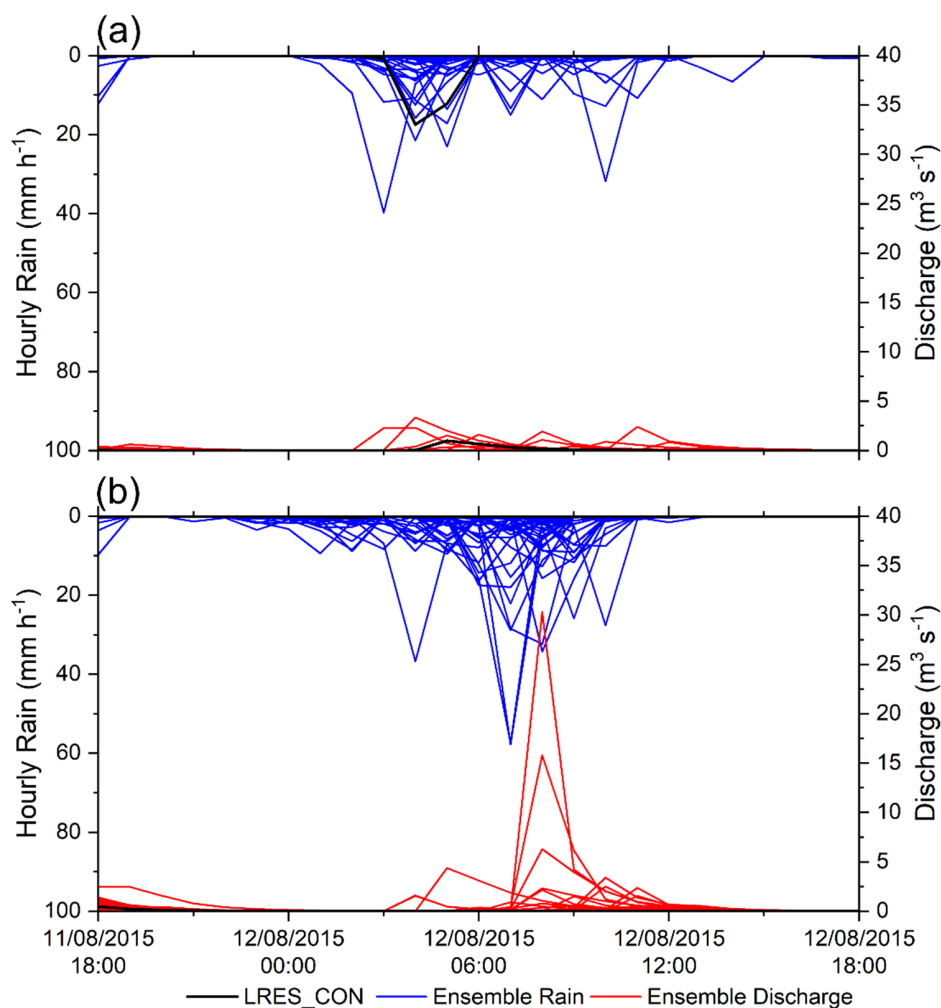


**Figure 8.** Hourly accumulated rainfall averaged over the Citrea creek catchment with the ensemble low-resolution control forecast and the 50 perturbed ensemble forecasts, and resulting hydrographs: (a) forecasts starting at 0000 UTC, 11 August 2015; (b) forecasts starting at 1200 UTC, 11 August 2015.

Overall, none of the members of the ensembles seems able to contribute to completely reliable hydrological forecasts at the resolution of the small catchment analyzed, even though many of them can warn about the probability of a significant hydrological impact considering a wider area, and some of them can even forecast a significant flow increase for the analyzed 11.4 km<sup>2</sup> wide catchment.

#### 4. Discussion and Conclusions

The objective of a quantitatively accurate assessment of the hydrometeorological impact at the resolution of the small and very small coastal Mediterranean catchments is still a too demanding challenge for the current level of development of forecasting techniques. This awareness leads the Italian National Civil Protection agency to a strategy based on the definition of relatively wide warning areas, whose extents are indicative of the maximum resolution to go for assumed by operational agencies, to have reliable forecasts in an operating context. Specifically, the Calabria region is divided into eight warning areas almost 2000 km<sup>2</sup> wide on average, and the Corigliano area falls in that to the north-east.

The analyzed event has specific features that make its accurate forecast particularly difficult: Highly convective dynamics, very localized impact on the ground both in time and (mainly) in space, and a morphologically complex area with complex air–sea interactions. Based on this test case, we argue that, within the current operational framework based on warning areas of the order of 10<sup>3</sup> km<sup>2</sup>, the dynamical downscaling approach based on an ensemble forecast strategy can provide further useful information for the correct detection of the hydrological effects even for such particular events. Most of the ensemble members amplify and localize the larger-scale signal provided by the GCM, supplying indications about the spots, within the warning area, where the impact on the ground is most probable. The output of the ensemble forecasts can be communicated in a relatively straightforward way by employing percentile maps, such as those shown in Figures 3d and 4d, which, together with the quantitative information, also provide a measure of the forecast uncertainty. Furthermore, in the analyzed test case, the ensemble forecast starting closer to the occurrence time of the event (i.e., the simulation starting at 1200 UTC with a lower lead time) provides more accurate predictions of rainfall intensity and, partially, of its location (Figure 5b), reaching in few but significant cases also an accurate hydrological forecast in the small catchment under analysis (Figure 8b).

Regarding the main aim of this study, i.e., the assessment of the benefit of an ensemble approach on the predictability of a highly localized convective event (and related hydrological impact) in the Mediterranean area, the analyzed test case leads to some generalizable conclusions, i.e.:

1. In orographically complex areas, prone to high-impact very localized weather events, such as it is the case for most of the mountainous Mediterranean coasts, an ensemble approach should be preferred to single-based simulations, even if at the cost of a higher calculation burden, given its capability of improving forecast skills in terms of both rainfall intensity and location;
2. The higher information content offered by an ensemble system can be managed through percentile maps, which facilitate the interpretation of the forecast uncertainty in space and highlight the sub-zones, within the warning areas, most likely subject to risk; and
3. Such management of the forecast uncertainty can be very useful for operational purposes, being capable, in principle, to support civil protection actions that, though activated in the whole warning area, can start to prepare more targeted actions for specific sub-zones.

Furthermore, this case study demonstrates that by reducing the forecast horizon, the ensemble forecast can be very accurate up to the hydrological impact also on a coastal catchment about 10 km<sup>2</sup> wide.

The experiment performed gives hints also about the limits of the proposed approach. From an operational point of view, it is noteworthy that, according to the results of the ensemble simulation, the Corigliano area is highlighted as a possible hotspot of the event together with a couple of other well-localized areas, where, however, false alarms would have been issued. Furthermore, the local

morphology, entailing a subdivision of the territory into many small basins, does not allow in any case to attribute a completely reliable rainfall rate (and the corresponding hydrological response) to the catchment that was most affected. From a scientific point of view, instead, it is interesting that the accuracy of the forecast is not enhanced by the higher-resolution (16 km vs. 32 km) boundary conditions provided by the high-resolution ECMWF IFS simulation, such as Figure 6 highlights. This result has to be connected to the small-scale and intrinsically chaotic properties of the convective event, which can hide possible positive effects of improved initial and/or boundary conditions [33] and whose predictability can be addressed only in terms of the average behavior [60]. Convective storms forecasting is still a significantly evolving research field, which involves both theoretical and observational aspects [61].

The research presented in this paper shows an assessment strategy outlined for a specific, though exemplary, event. Many options are possible for strengthening the results achieved. Beyond taking into consideration more episodes, either convective or caused by frontal systems, which would expand the range of test cases and the related performance of the ensemble simulations, also going into details regarding the issue of predictability of a single event at different lead times is of particular interest from a civil protection point of view, given the importance of the time available to implement defense measures. Furthermore, the investigation on uncertainty can be expanded by considering also the issues connected to the initialization of the hydrological models, among which the soil moisture conditions are included (e.g., [17,62–64]). All these research lines, however, must deal with a higher computational burden, which could represent a strong constraint to the development of such systems in operational contexts. From this point of view, for example, the ensemble forecast starting at 1200 UTC could be useless in practice, due to the high number of simulations to perform in a very short time before the occurrence of the event. Therefore, the good results achieved up to the hydrological forecast in a very small catchment could have no positive impact in an operational modelling chain. To reduce this problem, looking for effective ensemble strategies (e.g., [65,66]) could help while waiting for the further increase of efficiency of parallel computing systems. On the other hand, complementary strategies for improving the forecast accuracy with a longer lead time can be based on both ensemble forecasts and data assimilation (e.g., [67,68]). Even the impact on the ground can be assessed through innovative approaches dealing with uncertainties, like [69], that is particularly useful for highly localized events.

Finally, while studying the potential of convection-permitting ensemble systems, the very rapid improvement of the GCMs providing the boundary conditions must be taken into account. For example, in 2016, the year after the occurrence of the analyzed event, both the ECMWF IFS and EPS resolutions increased a lot, in the framework of an overall forecasting system upgrade that provided other improvements as well. Therefore, for a state-of-the-art assessment of the predictability of complex convection-permitting hydro-meteorological (either single or probabilistic) forecasting systems, it makes sense to focus not only on the most up-to-date modelling systems but also, when possible, on recent events.

**Author Contributions:** Conceptualization, A.S. and G.M.; methodology and validation, L.F., G.M. and A.S.; formal analysis, L.F.; investigation, L.F.; writing—original draft preparation, A.S.; writing—review and editing, L.F., G.M. and A.S.; visualization, L.F. and A.S.; supervision, G.M. All authors have read and agreed to the published version of the manuscript.

**Funding:** The activity of L. Furnari was founded by the Programme “POR Calabria FSE/FESR 2014/2020—Mobilità internazionale di Dottorandi e Assegnisti di ricerca/Ricercatori di Tipo A” Actions 10.5.6 and 10.5.12.

**Acknowledgments:** Authors thank the Italian National Civil Protection “Centro Funzionale Centrale Rischio Meteo-idrogeologico e Idraulico” for providing radar data, and the “Centro Funzionale Multirischi” of the Calabrian Regional Agency for the Protection of the Environment (ARPACAL) for providing the observed precipitation data. This work is a contribution to the HyMeX international programme.

**Conflicts of Interest:** The authors declare no conflict of interest.

## References

1. Pagano, T.C.; Wood, A.W.; Ramos, M.H.; Cloke, H.L.; Pappenberger, F.; Clark, M.P.; Cranston, M.; Kavetski, D.; Mathevet, T.; Sorooshian, S.; et al. Challenges of operational river forecasting. *J. Hydrometeorol.* **2014**, *15*, 1692–1707. [CrossRef]
2. Buizza, R. Chapter 2-Ensemble Forecasting and the Need for Calibration. In *Statistical Postprocessing of Ensemble Forecasts*; Vannitsem, S., Wilks, D.S., Messner, J.W., Eds.; Elsevier: Amsterdam, The Netherlands, 2018; pp. 15–48. ISBN 9780128123720.
3. Renard, B.; Kavetski, D.; Kuczera, G.; Thyer, M.; Franks, S.W. Understanding predictive uncertainty in hydrologic modelling: The challenge of identifying input and structural errors. *Water Resour. Res.* **2010**, *46*, W05521. [CrossRef]
4. Clark, P.; Roberts, N.; Lean, H.; Ballard, S.P.; Charlton-Perez, C. Convection-permitting models: A step-change in rainfall forecasting. *Meteorol. Appl.* **2016**, *23*, 165–181. [CrossRef]
5. Palmer, T. The ECMWF ensemble prediction system: Looking back (more than) 25 years and projecting forward 25 years. *Q. J. R. Meteorol. Soc.* **2019**, *145* (Suppl. 1), 12–24. [CrossRef]
6. Palmer, T.N.; Molteni, F.; Mureau, R.; Buizza, R.; Chapelet, P.; Tribbia, J. Ensemble Prediction. ECMWF Technical Memorandum No. 188. 1992. Available online: <https://www.ecmwf.int/en/elibrary/11560-ensemble-prediction> (accessed on 27 May 2020).
7. Evans, C.; Dyke, D.; Lericos, T. How Do Forecasters Utilize Output from a Convection-Permitting Ensemble Forecast System? Case Study of a High-Impact Precipitation Event. *Weather Forecast.* **2014**, *29*, 466–486. [CrossRef]
8. Baker, L.H.; Rudd, A.C.; Migliorini, S.; Bannister, R.N. Representation of model error in a convective-scale ensemble prediction system. *Nonlinear Process. Geophys.* **2014**, *21*, 19–39. [CrossRef]
9. Dey, S.R.; Plant, R.S.; Roberts, N.M.; Migliorini, S. Assessing spatial precipitation uncertainties in a convective-scale ensemble. *Q. J. R. Meteorol. Soc.* **2016**, *142*, 2935–2948. [CrossRef]
10. Nuissier, O.; Marsigli, C.; Vincendon, B.; Hally, A.; Bouttier, F.; Montani, A.; Paccagnella, T. Evaluation of two convection-permitting ensemble systems in the HyMeX Special Observation Period (SOP1) framework. *Q. J. R. Meteorol. Soc.* **2016**, *142*, 404–418. [CrossRef]
11. Schellander-Gorgas, T.; Wang, Y.; Meier, F.; Weidle, F.; Wittmann, C.; Kann, A. On the forecast skill of a convection-permitting ensemble. *Geosci. Model Dev.* **2017**, *10*, 35–56. [CrossRef]
12. Ma, S.; Chen, C.; He, H.; Wu, D.; Zhang, C. Assessing the Skill of Convection-Allowing Ensemble Forecasts of Precipitation by Optimization of Spatial-Temporal Neighborhoods. *Atmosphere* **2018**, *9*, 43. [CrossRef]
13. Gowan, T.M.; Steenburgh, W.J.; Schwartz, C.S. Validation of Mountain Precipitation Forecasts from the Convection-Permitting NCAR Ensemble and Operational Forecast Systems over the Western United States. *Weather Forecast.* **2018**, *33*, 739–765. [CrossRef]
14. Hally, A.; Richard, E.; Ducrocq, V. An ensemble study of HyMeX IOP6 and IOP7a: Sensitivity to physical and initial and boundary condition uncertainties. *Nat. Hazards Earth Syst. Sci.* **2014**, *14*, 1071–1084. [CrossRef]
15. Johnson, A.; Wang, X. A Study of Multiscale Initial Condition Perturbation Methods for Convection-Permitting Ensemble Forecasts. *Mon. Weather Rev.* **2016**, *144*, 2579–2604. [CrossRef]
16. Keresturi, E.; Wang, Y.; Meier, F.; Weidle, F.; Wittmann, C.; Atencia, A. Improving initial condition perturbations in a convection-permitting ensemble prediction system. *Q. J. R. Meteorol. Soc.* **2019**, *145*, 993–1012. [CrossRef]
17. Zappa, M.; Jaun, S.; Germann, U.; Walser, A.; Fundel, F. Superposition of three sources of uncertainties in operational flood forecasting chains. *Atmos. Res.* **2011**, *100*, 246–262. [CrossRef]
18. Calvetti, L.; Pereira Filho, A.J. Ensemble Hydrometeorological Forecasts Using WRF Hourly QPF and TopModel for a Middle Watershed. *Adv. Meteorol.* **2014**, *2014*, 484120. [CrossRef]
19. Golding, B.; Roberts, N.; Leoncini, G.; Mylne, K.; Swinbank, R. MOGREPS-UK Convection-Permitting Ensemble Products for Surface Water Flood Forecasting: Rationale and First Results. *J. Hydrometeors* **2016**, *17*, 1383–1406. [CrossRef]
20. Saleh, F.; Ramaswamy, V.; Georgas, N.; Blumberg, A.F.; Pullen, J. A retrospective streamflow ensemble forecast for an extreme hydrologic event: A case study of Hurricane Irene and on the Hudson River basin. *Hydrol. Earth Syst. Sci.* **2016**, *20*, 2649–2667. [CrossRef]

21. Olsson, J.; Pers, B.C.; Bengtsson, L.; Pechlivanidis, I.; Berg, P.; Körnich, H. Distance-dependent depth-duration analysis in high-resolution hydro-meteorological ensemble forecasting: A case study in Malmö City, Sweden. *Environ. Model. Softw.* **2017**, *93*, 381–397. [[CrossRef](#)]
22. Giorgi, F. Climate change hot-spots. *Geophys. Res. Lett.* **2006**, *33*, L08707. [[CrossRef](#)]
23. Scoccimarro, E.; Villarini, G.; Vichi, M.; Zampieri, M.; Fogli, P.G.; Bellucci, A.; Gualdi, S. Projected Changes in Intense Precipitation over Europe at the Daily and Subdaily Time Scales. *J. Clim.* **2015**, *28*, 6193–6203. [[CrossRef](#)]
24. Drobinski, P.; Silva, N.D.; Panthou, G.; Bastin, S.; Muller, C.; Ahrens, B.; Borga, M.; Conte, D.; Fosser, G.; Giorgi, F.; et al. Scaling precipitation extremes with temperature in the Mediterranean: Past climate assessment and projection in anthropogenic scenarios. *Clim. Dyn.* **2018**, *51*, 1237–1257. [[CrossRef](#)]
25. Vié, B.; Molinié, G.; Nuissier, O.; Vincendon, B.; Ducrocq, V.; Bouttier, F.; Richard, E. Hydro-meteorological evaluation of a convection-permitting ensemble prediction system for Mediterranean heavy precipitating events. *Nat. Hazards Earth Syst. Sci.* **2012**, *12*, 2631–2645. [[CrossRef](#)]
26. Davolio, S.; Miglietta, M.M.; Diomede, T.; Marsigli, C.; Montani, A. A flood episode in northern Italy: Multi-model and single-model mesoscale meteorological ensembles for hydrological predictions. *Hydrol. Earth Syst. Sci.* **2013**, *17*, 2107–2120. [[CrossRef](#)]
27. Hally, A.; Caumont, O.; Garrote, L.; Richard, E.; Weerts, A.; Delogu, F.; Fiori, E.; Rebora, N.; Parodi, A.; Mihalović, A.; et al. Hydrometeorological multi-model ensemble simulations of the 4 November 2011 flash flood event in Genoa, Italy, in the framework of the DRIHM project. *Nat. Hazards Earth Syst. Sci.* **2015**, *15*, 537–555. [[CrossRef](#)]
28. Corazza, M.; Sacchetti, D.; Antonelli, M.; Drofa, O. The ARPAL operational high resolution Poor Man's Ensemble, description and validation. *Atmos. Res.* **2018**, *203*, 1–15. [[CrossRef](#)]
29. Petrucci, O.; Salvati, P.; Aceto, L.; Bianchi, C.; Pasqua, A.A.; Rossi, M.; Guzzetti, F. The Vulnerability of People to Damaging Hydrogeological Events in the Calabria Region (Southern Italy). *Int. J. Environ. Res. Public Health* **2018**, *15*, 48. [[CrossRef](#)]
30. Gochis, D.J.; Yu, W.; Yates, D.N. The WRF-Hydro Model Technical Description and User's Guide, Version 3.0. NCAR Technical Document. 120 Pages. 2015. Available online: [http://www.ral.ucar.edu/projects/wrf\\_hydro/](http://www.ral.ucar.edu/projects/wrf_hydro/) (accessed on 27 May 2020).
31. Skamarock, W.C.; Klemp, J.B.; Dudhia, J.; Gill, D.O.; Barker, D.M.; Duda, M.G.; Huang, X.-Y.; Wang, W.; Powers, J.G. *A Description of the Advanced Research WRF Version 3*; NCAR Tech. Note NCAR/TN-475+STR: Boulder, CO, USA, 2008; p. 113.
32. Cloke, H.L.; Pappenberger, F. Ensemble flood forecasting: A review. *J. Hydrol.* **2009**, *375*, 613–626. [[CrossRef](#)]
33. Senatore, A.; Furnari, L.; Mendicino, G. Impact of improved Sea Surface Temperature representation on the forecast of small Mediterranean catchments hydrological response to heavy precipitation. *Hydrol. Earth Syst. Sci.* **2020**, *24*, 269–291. [[CrossRef](#)]
34. Federico, S.; Bellecci, C.; Colacino, M. Numerical simulation of Crotona flood: Storm evolution. *Il Nuovo Cim.* **2003**, *26*, 357–371.
35. Federico, S.; Avolio, E.; Bellecci, C.; Lavagnini, A.; Colacino, M.; Walko, R.L. Numerical analysis of an intense rainstorm occurred in southern Italy. *Nat. Hazards Earth Syst. Sci.* **2008**, *8*, 19–35. [[CrossRef](#)]
36. Chiaravalloti, F.; Gabriele, S. Vibo Valentia flood and MSG rainfall evaluation. *Atmos. Res.* **2009**, *93*, 286–294. [[CrossRef](#)]
37. Gascón, E.; Laviola, S.; Merino, A.; Miglietta, M.M. Analysis of a localized flash-flood event over the central Mediterranean. *Atmos. Res.* **2016**, *182*, 256–268. [[CrossRef](#)]
38. Avolio, E.; Federico, S. WRF simulations for a heavy rainfall event in southern Italy: Verification and sensitivity tests. *Atmos. Res.* **2018**, *209*, 14–35. [[CrossRef](#)]
39. Avolio, E.; Cavalcanti, O.; Furnari, L.; Senatore, A.; Mendicino, G. Brief communication: Preliminary hydro-meteorological analysis of the flash flood of 20 August 2018 in Raganello Gorge, southern Italy. *Nat. Hazards Earth Syst. Sci.* **2019**, *19*, 1619–1627. [[CrossRef](#)]
40. Senatore, A.; Mendicino, G.; Knoche, H.R.; Kunstmann, H. Sensitivity of Modeled Precipitation to Sea Surface Temperature in Regions with Complex Topography and Coastlines: A Case Study for the Mediterranean. *J. Hydrometeors* **2014**, *15*, 2370–2396. [[CrossRef](#)]
41. Chen, S.H.; Sun, W.H. A One-dimensional Time Dependent Cloud Model. *J. Meteorol. Soc. Jpn.* **2002**, *80*, 99–118. [[CrossRef](#)]

42. Mellor, G.L.; Yamada, T. Development of a turbulence closure model for geophysical fluid problems. *Rev. Geophys.* **1982**, *20*, 851–875. [[CrossRef](#)]
43. Dudhia, J. Numerical Study of Convection Observed during the Winter Monsoon Experiment Using a Mesoscale Two-Dimensional Model. *J. Atmos. Sci.* **1989**, *46*, 3077–3107. [[CrossRef](#)]
44. Mlawer, E.J.; Taubman, S.J.; Brown, P.D.; Iacono, M.J.; Clough, S.A. Radiative transfer for inhomogeneous atmospheres: RRTM, a validated correlated-k model for the longwave. *J. Geophys. Res.* **1997**, *102*, 16663–16682. [[CrossRef](#)]
45. Tewari, M.; Chen, F.; Wang, W.; Dudhia, J.; LeMone, M.A.; Mitchell, K.; Ek, M.; Gayno, G.; Wegiel, J.; Cuenca, R.H. Implementation and verification of the unified NOAA land surface model in the WRF model. In Proceedings of the 20th Conference on Weather Analysis and Forecasting/16th Conference on Numerical Weather Prediction, Seattle, WA, USA, 12–16 January 2004; pp. 11–15.
46. Janjić, Z.I. The Step-Mountain Eta Coordinate Model: Further Developments of the Convection, Viscous Sublayer, and Turbulence Closure Schemes. *Mon. Weather Rev.* **1994**, *122*, 927–945. [[CrossRef](#)]
47. Kain, J.S. The Kain–Fritsch Convective Parameterization: An Update. *J. Appl. Meteorol.* **2004**, *43*, 170–181. [[CrossRef](#)]
48. ECMWF (European Centre for Medium-Range Weather Forecasts). IFS Documentation Cy41r1 Operational Implementation 12 May 2015, Part V: Ensemble Prediction System. 2015. Available online: <https://www.ecmwf.int/sites/default/files/elibrary/2015/9212-part-v-ensemble-prediction-system.pdf> (accessed on 27 May 2020).
49. Leutbecher, M.; Palmer, T.N. Ensemble forecasting. *J. Comput. Phys.* **2008**, *227*, 3515–3539. [[CrossRef](#)]
50. Merchant, C.J.; Filippiak, M.J.; Le Borgne, P.; Roquet, H.; Autret, E.; Piollé, J.-F.; Lavender, S. Diurnal warm-layer events in the western Mediterranean and European shelf seas. *Geophys. Res. Lett.* **2008**, *35*, L04601. [[CrossRef](#)]
51. Robinson, I.; Piolle, J.F.; Leborgne, P.; Poulter, D.; Donlon, C.; Arino, O. Widening the application of AATSR SST data to operational tasks through the Medspiration Service. *Remote Sens. Environ.* **2012**, *116*, 126–139. [[CrossRef](#)]
52. Zeng, X.; Beljaars, A. A prognostic scheme of sea surface skin temperature for modelling and data assimilation. *Geophys. Res. Lett.* **2009**, *32*, L14605.
53. Gochis, D.J.; Barlage, M.; Dugger, A.; FitzGerald, K.; Karsten, L.; McAllister, M.; McCreight, J.; Mills, J.; RafieeiNasab, A.; Read, L.; et al. *The WRF-Hydro Modeling System Technical Description, (Version 5.0)*; NCAR Technical Note: Boulder, CO, USA, 2018; p. 107. Available online: [https://ral.ucar.edu/sites/default/files/public/WRF-HydroV5TechnicalDescription\\_update512019\\_0.pdf](https://ral.ucar.edu/sites/default/files/public/WRF-HydroV5TechnicalDescription_update512019_0.pdf) (accessed on 9 April 2020).
54. Yucel, I.; Onen, A.; Yilmaz, K.K.; Gochis, D.J. Calibration and Evaluation of a Flood Forecasting System: Utility of Numerical Weather Prediction Model, Data Assimilation and Satellite-Based Rainfall. *J. Hydrol.* **2015**, *523*, 49–66. [[CrossRef](#)]
55. Senatore, A.; Mendicino, G.; Gochis, D.J.; Yu, W.; Yates, D.N.; Kunstmann, H. Fully coupled atmosphere-hydrology simulations for the central Mediterranean: Impact of enhanced hydrological parameterization for short and long time scales. *J. Adv. Modeling Earth Syst.* **2015**, *7*, 1693–1715. [[CrossRef](#)]
56. Givati, A.; Gochis, D.; Rummeler, T.; Kunstmann, H. Comparing One-Way and Two-Way Coupled Hydrometeorological Forecasting Systems for Flood Forecasting in the Mediterranean Region. *Hydrology* **2016**, *3*, 19. [[CrossRef](#)]
57. CFM (Centro Funzionale Multirischi della Calabria). Technical Report, Rapporto Speditivo di Evento Meteopluviometrico del 12 Agosto 2015 (In Italian). 2015. Available online: <http://www.cfd.calabria.it/DatiVari/Pubblicazioni/rapporto%20di%20evento%2012%20agosto.pdf> (accessed on 27 May 2020).
58. ISPRA. *Territorio. Processi e Trasformazioni in Italia*; ISPRA: Roma, Italy, 2018; p. 296. ISBN 978-88-448-0921-8. Available online: <http://www.isprambiente.gov.it/it/pubblicazioni/rapporti/territorio-processi-e-trasformazioni-in-italia> (accessed on 27 May 2020).
59. Dee, D.P.; Uppala, S.M.; Simmons, A.J.; Berrisford, P.; Poli, P.; Kobayashi, S.; Andrae, U.; Balmaseda, M.A.; Balsamo, G.; Bauer, P.; et al. The ERA-Interim reanalysis: Configuration and performance of the data assimilation system. *Q. J. R. Meteorol. Soc.* **2011**, *137*, 553–597. [[CrossRef](#)]
60. Raymond, D.; Fuchs, Ž.; Gjorgjievskaja, S.; Sessions, S. Balanced dynamics and convection in the tropical troposphere. *J. Adv. Modeling Earth Syst.* **2015**, *7*, 1093–1116. [[CrossRef](#)]

61. Brooks, H.E.; Doswell, C.A., III; Zhang, X.; Chernokulsky, A.M.; Tochimoto, E.; Hanstrum, B.; de Lima Nascimento, E.; Sills, D.M.; Antonescu, B.; Barrett, B. A Century of Progress in Severe Convective Storm Research and Forecasting. *Meteorol. Monogr.* **2018**, *59*, 18.1–18.41. [[CrossRef](#)]
62. Edouard, S.; Vincendon, B.; Ducrocq, V. Ensemble-based flash-flood modelling: Taking into account hydrodynamic parameters and initial soil moisture uncertainties. *J. Hydrol.* **2018**, *560*, 480–494. [[CrossRef](#)]
63. Li, L.; Pontoppidan, M.; Sobolowski, S.; Senatore, A. The impact of initial conditions on convection-permitting simulations of a flood event over complex mountainous terrain. *Hydrol. Earth Syst. Sci.* **2020**, *24*, 771–791. [[CrossRef](#)]
64. Fersch, B.; Senatore, A.; Adler, B.; Arnault, J.; Mauder, M.; Schneider, K.; Völksch, I.; Kunstmann, H. High-resolution fully-coupled atmospheric–hydrological modeling: A cross-compartment regional water and energy cycle evaluation. *Hydrol. Earth Syst. Sci.* **2020**, *24*, 2457–2481. [[CrossRef](#)]
65. Ravazzani, G.; Amengual, A.; Ceppi, A.; Homar, V.; Romero, R.; Lombardi, G.; Mancini, M. Potentialities of ensemble strategies for flood forecasting over the Milano urban area. *J. Hydrol.* **2016**, *539*, 237–253. [[CrossRef](#)]
66. Roux, H.; Amengual, A.; Romero, R.; Bladé, E.; Sanz-Ramos, M. Evaluation of two hydrometeorological ensemble strategies for flash-flood forecasting over a catchment of the eastern Pyrenees. *Nat. Hazards Earth Syst. Sci.* **2020**, *20*, 425–450. [[CrossRef](#)]
67. Munsell, E.B.; Zhang, F. Prediction and uncertainty of Hurricane Sandy (2012) explored through a real-time cloud-permitting ensemble analysis and forecast system assimilating airborne Doppler radar observations. *J. Adv. Modeling Earth Syst.* **2014**, *6*, 38–58. [[CrossRef](#)]
68. Yussouf, N.; Dowell, D.C.; Wicker, L.J.; Knopfmeier, K.H.; Wheatley, D.M. Storm-scale data assimilation and ensemble forecasts for the 27 April 2011 severe weather outbreak in Alabama. *Mon. Weather Rev.* **2015**, *143*, 3044–3066. [[CrossRef](#)]
69. Lombardi, G.; Ceppi, A.; Ravazzani, G.; Davolio, S.; Mancini, M. From Deterministic to Probabilistic Forecasts: The ‘Shift-Target’ Approach in the Milan Urban Area (Northern Italy). *Geosciences* **2018**, *8*, 181. [[CrossRef](#)]



© 2020 by the authors. Licensee MDPI, Basel, Switzerland. This article is an open access article distributed under the terms and conditions of the Creative Commons Attribution (CC BY) license (<http://creativecommons.org/licenses/by/4.0/>).